metals

MDPI

Review

Review of Characterization on Hydrogen Embrittlement by Micro-Sample Testing Methods

Ping Tao [1,2,*], Wei Zhou [1,2], Xinting Miao [1,2], Jian Peng [1,2] and Wenming Liu [1,2]

[1] School of Mechanical Engineering and Rail Transit, Changzhou University, Changzhou 213164, China
[2] Jiangsu Key Laboratory of Green Process Equipment, Changzhou University, Changzhou 213164, China
* Correspondence: pingtao@cczu.edu.cn

Abstract: Conventional-sized specimens have been well and widely applied in research on hydrogen embrittlement. However, when the limited-size core components (nozzles and valves, etc.) of hydrogen energy equipment are evaluated for service damage, traditional testing with conventional-sized samples is no longer applicable and micro-sample testing methods are required. In this paper, recent progress in the characterization of hydrogen embrittlement achieved via a small-sized sample tensile test, small punch test and nanoindentation test is reviewed. The commonly used geometries and dimensions of various small-sized specimens are first described and the in situ hydrogen-containing environment testing cases equipped with small-sized specimens are presented, proving the advantages of direct observations of hydrogen influences on the mechanical property and microstructure evolution. Then, the quantitative analysis of hydrogen embrittlement sensitivity involving a small punch test is discussed, with a focus on the comparisons of the hydrogen embrittlement index calculated using different definition methods. Finally, the nanoindentation test of investigation on the interaction between hydrogen and dislocation in metals and the effect of indentation strain rate are summarized. Furthermore, the specific research directions and applications of micro-size specimens for further investigation on hydrogen embrittlement are identified.

Keywords: hydrogen embrittlement; small-size tensile; small punch test; nanoindentation

Citation: Tao, P.; Zhou, W.; Miao, X.; Peng, J.; Liu, W. Review of Characterization on Hydrogen Embrittlement by Micro-Sample Testing Methods. *Metals* **2023**, *13*, 1753. https://doi.org/10.3390/met13101753

Academic Editor: Jin-Yoo Suh

Received: 24 September 2023
Revised: 9 October 2023
Accepted: 11 October 2023
Published: 16 October 2023

1. Background and Introduction

In the context of tackling global environmental pollution and climate warming, hydrogen energy has been considered as a promising fuel for the low-carbon transformation of global energy resources, with its advantages of cleanliness, flexibility and efficiency, and its wide variety of sources and applications. Most countries have listed hydrogen energy as a priority area of frontier technology and industrial transformation. Along with the maturity of terminal application of hydrogen energy, e.g., hydrogen fuel cell, a large number of metallic structures, including hydrogen storage, hydrogen transport and hydrogenation pressure vessels and pipelines, have been continuously built. However, it has been found that the metallic materials are prone to premature brittle failure when they are served in a hydrogen-containing environment, known as hydrogen embrittlement (HE) [1–3]. Because of the low density, low ignition points and wide-range explosions caused by hydrogen, the failure of hydrogen storage and transport vessels will result in serious consequences. Therefore, ensuring the structural integrity of hydrogen energy equipment has become a key issue that needs to be solved in the further promotion and application of hydrogen energy [4,5].

HE research has been focused on for nearly 150 years, and many scholars have carried out hydrogen–metal compatibility studies. The existing research results are of great significance to the economic and safe use of energy and chemical equipment materials, such as carbon steel, low-alloy steel, stainless steel and titanium alloy, etc. The failure modes of many equipment or components (such as low-temperature brittleness, delayed

failure, fatigue, creep and stress corrosion rupture, etc.) are related to the promotion of hydrogen. HE refers to the phenomenon that hydrogen interacts with the metal matrix, causing mechanical properties such as toughness and plasticity to decline as well as resulting in brittle or cracking of the material. It can usually be divided into two categories: (i) Internal Hydrogen Embrittlement (IHE) and (ii) Environmental Hydrogen Embrittlement (EHE). IHE indicates that hydrogen has entered the metal before force deformation has occurred through the process of smelting, pickling, electroplating, etc. EHE refers to the case in which entry of hydrogen is accompanied by the stress deformation of the metal, which is usually directed to the service in a hydrogen-related environment [6,7]. Although there is no essential difference between IHE and EHE in the final mechanism, the process, degree and form of the damage may be different. In some cases, internal hydrogen damage and environmental damage occur simultaneously, leading to the deformation of the hydrogen-absorbed metal in the hydrogen environment.

So far, although many HE theories have been proposed, they are still not unified. The reason is that the hydrogen diffusion, dissolution, and trapping characteristics of different crystal structure materials are not the same. At present, HE theories related to metal materials mainly include [8,9]: (i) Hydrogen Pressure—HP; (ii) Hydride Theory—HT; (iii) Dislocation Interaction—DI; (iv) Hydrogen-Enhanced Decohesion—HEDE; (v) Hydrogen-Enhanced Local Plasticity—HELP; (vi) the Synergy theory of HEDE and HELP—HEDE + HELP; (vii) Hydrogen Absorption-Induced Dislocation Emission—HAIDE; (viii) Hydrogen-Enhanced Strain-Induced Vacancies—HESIV. According to different application scenes, each HE theory has its own limitations, more or less, so it needs to be comprehensively analyzed according to the actual situation. HEDE theory, HELP theory as well as HEDE + HELP synergistic theory are widely accepted and used in the study of the HE phenomenon of commonly used steels. According to the HEDE theory [10,11], hydrogen reduces the bonding force (also known as cohesion) between metal atoms, which leads to the separation of metal atoms under low tensile stress, causing crack nucleation, initiation and expansion. The HELP theory indicates that hydrogen atoms will increase the mobility of the dislocation in the region near the crack tip, resulting in "local softening" of the material. When the plastic deformation caused by this "local softening" accumulates to a critical state, it will cause the nucleation of micro-cracks, resulting in premature failure of the material. Unlike the HEDE theory, in the HELP theory, the plasticity of the material plays an important role in hydrogen-induced fracture [12,13]. The HELP + HEDE theory believes that several HE mechanisms are more likely to act simultaneously. In most cases of hydrogen-induced cracking, one HE mechanism usually dominates. It is also possible that initially only one HE mechanism (such as HELP) dominates, but later another HE mechanism (such as HEDE) dominates due to environmental changes in the service. To date, several mechanisms of the synergistic effect of HE mechanisms have been gradually recognized [14,15].

The quantitative difference between the mechanical properties of metals with and without hydrogen is used to evaluate the degree of hydrogen influence, i.e., HE sensitivity. The commonly used standard dimensional tensile test methods include the smooth tensile test and the notch tensile test. Studies have shown that the effect of hydrogen on material strength is usually inconspicuous, which mainly reduces the elongation and section shrinkage, referred to as hydrogen-induced ductility loss. Therefore, the elongation or reduction in the area is usually used to measure the HE sensitivity in the smooth tensile test [16,17]. The stress state of the sample in the smooth tensile test is the uniaxial stress state before necking, but the actual structure often has geometric discontinuous dimension, such as notch due to metallurgy, processing or structural needs, leading to the stress concentration in front of the notch, which is mostly close to the state of multi-axial stress. For this reason, the tensile test of notched samples is also often used to investigate the HE sensitivity [18,19]. In general, the notched specimens exhibit greater ductility loss than smooth specimens [20,21].

It has been shown that the research on HE damages and mechanisms based on conventional-sized specimens is remarkable. However, when evaluating the service damage of core components with limited size, such as nozzles and valves, the traditional test methods of conventional-sized samples are no longer applicable, and the micro-sample method is highly recommended. Since the 1960s, the micro-sample testing method has been applied to investigate the mechanical properties of materials. It was first used to assess the risk of embrittlement of pipelines and pressure vessels subjected to long-term neutron radiation in nuclear reactors. In recent years, with the development of structural refinement and miniaturization in industrial engineering applications such as aerospace, nuclear reactors, chemical equipment and instrumentation, small-sized components such as thin plates and thin-walled pipe fittings have been popularized and applied. It is of great significance to study the mechanical properties of materials obtained using the micro-size sample method, which is relevant to the needs of complex sampling and high-throughput, multi-parameter, and cross-scale testing in the development of new materials and service equipment. In terms of quantitative analysis of the mechanical properties and fracture behavior of materials induced by hydrogen, the micro-sample method has a small size, which can shorten the hydrogen charging time and facilitate the hydrogen charging and discharging test, making it a promising method for investigating HE [22–24]. In this paper, the study of micro-sample tensile test (MSTT), small punch test (SPT) and nanoindentation (NI) test are reviewed. The tensile test of standard-size sample is taken as a reference. Figure 1 shows the load–displacement (L-D) curves of uniaxial tensile test, small punch test and nanoindentation test.

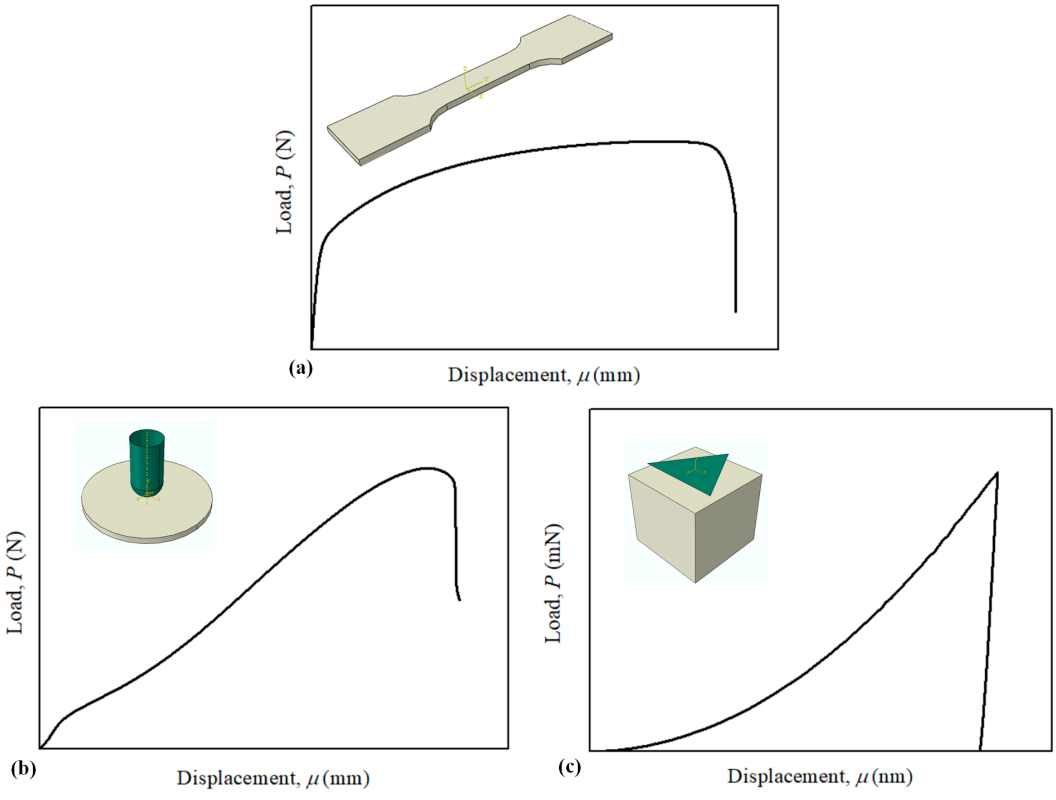

Figure 1. Comparisons of the load–displacement curves tested using (**a**) uniaxial tensile, (**b**) small punch and (**c**) nanoindentation tests of 316L steel.

The mechanical curves are all tested using the identical 316L austenitic stainless steel, which is convenient to directly compare here to the obtained L-D curves. It is seen that the obtained mechanical property curves of the SPT and NI test present the distinct characteristics of the uniaxial tensile test. The SPT and NI specimens show non-uniform

stress–strain distributions during deformation, and the results are unable to be compared directly with the standard tensile tests. At present, the empirical formula, reverse finite element modeling and machine learning method are commonly used. In reality, many studies have focused on the combination of multiple test methods, which can provide more comprehensive results for dealing with the mechanical degradation problem of metals in hydrogen-containing environments.

2. Micro-Sample Tensile Test and Hydrogen Embrittlement Characterization

2.1. Application of Small-Size Sample Tensile Test

Due to the limited volume and size of the structure and components to be measured, it is impossible to prepare test samples of conventional size. The micro-size samples are therefore essential. At present, micro-sample tensile testing methods have a wide range of applications in the engineering field, including (i) online inspection and life evaluation of in-service equipment, e.g., ageing equipment problems in nuclear power plant reactors; (ii) research and development of new materials, e.g., mechanical properties of nanomaterials, composites and precious metals; (iii) local-region mechanical properties analysis and damage behavior prediction of heterogeneous structures, e.g., heat-affected zones in weld joints and single-phase properties of multi-phase structures in steels; (iv) meso- and micro-scale mechanical behaviors, e.g., gradient materials, thin-film materials, biological materials, and microscopic devices. The schematic geometries of various small-sized specimens are shown from macro- to nano-scales in Figure 2 [25].

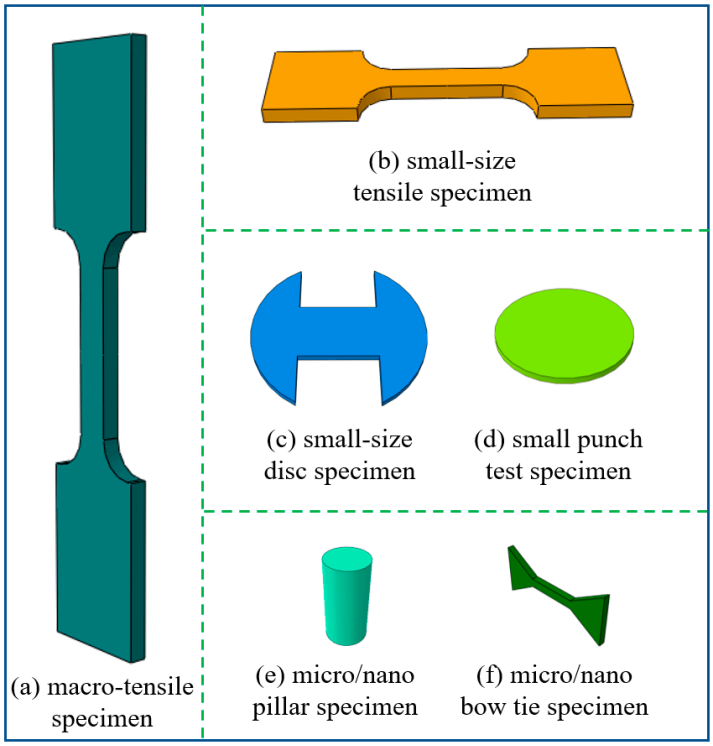

Figure 2. Schematic diagram of commonly used small-sized specimens.

Published studies have shown that the factors affecting the tensile test results of micro-samples include the cross-section diameter, thickness, length of parallel section in the middle of the sample and the grain size of the material. When the sample size is reduced from the conventional tensile sample, although the small-sized tensile test results are different from those of the conventional sample, they can be described by continuum mechanics, and the test results can still reflect the tensile properties of the material. Once the sample size reaches a certain critical value [26], the size effect of the sample is highlighted, and the tensile test results of the tiny sample cannot reflect the tensile properties of the

material itself. It is usually reflected by an insufficient number of grains in the sample thickness direction. The minimum applicable sample thickness is to be tens to hundreds of times the grain size [27,28]. The lack of characteristic microstructure within the sample or in the characteristic deformation region can cause the test results to deviate from the intrinsic macroscopic mechanical behavior of the tested material. Therefore, some size restrictions should be implemented to reduce or avoid the effects of size effect. For example, the ratio of thickness to the grain size of flat samples should not be less than 5–10 [29]. The minimum sizes of thickness and gauge length were recommended as 0.2 mm and 2 mm, respectively [25,30]. Small-sized specimens with different parallel lengths are shown in Figure 3, and they cover almost all possible options for the reduced aspect ratio (1:1 to 5:1) [31].

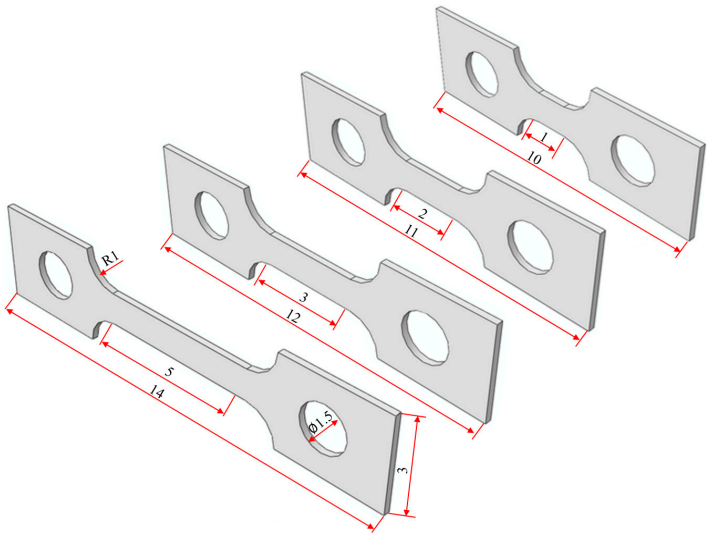

Figure 3. Small-sized specimens with different parallel lengths (unit: mm).

2.2. Hydrogen Embrittlement Characterization on Micro-Sample Tensile Test

With the rapid development of experimental testing technology, the tensile properties of small or micro samples are usually tested by placing them in the scanning electron microscope (SEM) or transmission electron microscope (TEM) chamber, which can realize the in situ testing of tensile mechanical properties and the characterization of microscopic morphology [32,33]. Many researchers have performed investigations of HE via micro-sample tensile tests owing to the in situ advanced equipment. T. Depover et al. [33] evaluated the HE sensitivity and related hydrogen-assisted crack initiation in transformation-induced plasticity (TRIP) steel. Unlike the electrochemically charged specimens, the plasma-charged specimens presented a ductility increase, and the crack initiation in the soft arresting ferritic matrix, whereas electrochemically charged specimens show crack initiation in the martensitic regions. Yoji Mine et al. [34] carried out micro-tensile tests on single- and twinned bi-crystals metastable 304 austenitic steel. It was concluded that the transformation of layered-structure martensite results in the effusion of excessive hydrogen dissolved in the original austenite phase. The high concentration of hydrogen concentrated in the remaining austenite between the martensite lamella leads to local shear of the residual austenite along the customary surface of martensitic transformation, resulting in quasi-cleavage fracture. M. Asadipoor et al. [35] investigated the mechanical properties of X70 pipeline steel using in situ H-plasma charging and ex situ electrochemical H-charging methods. Their research emphasized the methodological innovation of the plasma hydrogen charging technique. The in situ observations of hydrogen-induced effects, such as the formation of secondary cracks resulting from MnS and Al_2O_3 inclusions, and the transition of fracture features from ductile dimples to cleavage patterns was well presented. Shohei Ueki et al. [36] determined the effect of nano-twins on HE in the nano-twinned 304 steel. It was shown

that controlling the orientation and distribution of nano-twins can strengthen metastable austenitic steel and reduce the ductility loss caused by hydrogen. Based on the above-reported research, there is no doubt that the direct observations of microstructure evolution and crack initiation provide new insights into the HE phenomenon and a practical basis for the improvement of HE theory.

3. Small Punch Test and Hydrogen Embrittlement Sensitivity Analysis

3.1. Description of Small Punch Test

SPT was also first used to assess the risk of embrittlement of pipeline and pressure vessel materials exposed to long-term neutron radiation in nuclear reactors, the same as the micro-sample tensile test. On the one hand, the large sampling size of conventional samples easily causes destructive damage to the equipment, and it will cause secondary damage in the subsequent welding repair. On the other hand, due to the limited access to irradiated materials, the radioactivity will increase with the increase in sample size. The load–displacement curves of the materials were obtained using a small round specimen (Φ10 mm $\times$ 0.5 mm), which was punched at a constant loading rate (0.2~0.5 mm/min) [37–39]. After decades of development, SPT testing results can be associated with several mechanical properties of materials, such as yield strength and tensile strength [40,41], ductile-to-brittle transition temperature [42], fracture toughness [43], creep strength [44] and life prediction [45], etc., playing a positive auxiliary role in the aspects of material mechanical property testing, structural integrity assessment and damage fracture control.

Relevant standards [37–39] have been established to correlate the mechanical parameters of SPT and standard tensile tests, including SPT yield load vs. standard tensile yield strength, SPT maximum load vs. standard elongation after tensile failure, and SPT biaxial equivalent strain vs. section shrinkage of a standard tensile test specimen, etc. As shown in Figure 4, according to the different deformation forms of the sample, the load–displacement curve of SPT can be divided into five regions [46,47], i.e., I—the elastic stage, II—the elasto-plastic transition stage, III—the plastic bending section, IV—the film stretching stage, and V—the fracture failure stage.

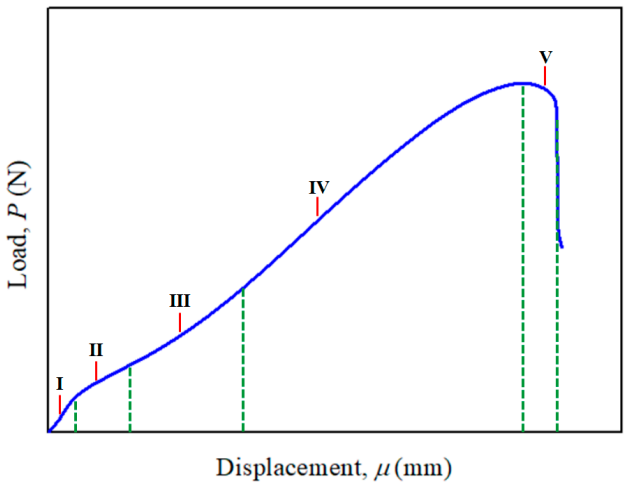

Figure 4. The divided five regions of load–displacement curve of small punch test.

The I and II stages are the main stages of elastoplastic deformation of the material, and the yield load (F_P) is generally defined according to the load value of the transition position of the I + II stage. However, due to the fact that the exact locations of the transition stages I and II cannot be directly determined, the selection criteria are not yet unified. Although different methods have been proposed [48], the yield loads obtained by these methods are different. As the yield load F_P is related to the final determined material mechanical property. It is necessary to determine a suitable and unified method to obtain F_P in order to accurately compare the differences in yield loads of different materials. Among them, the

method of extracting F_P by the least square method proposed by the European Committee Standard is often adopted [49], that is, the following two equations were obtained by using least square method at two points A and B (shown in Figure 5), after obtaining the load–displacement curve by SPT.

$$f(u) = \begin{cases} \frac{f_A}{u_A} u, & 0 \le u < u_A \\ \frac{f_B - f_A}{u_B - u_A} + f_A, & u_A \le u < u_B \end{cases} \quad (1)$$

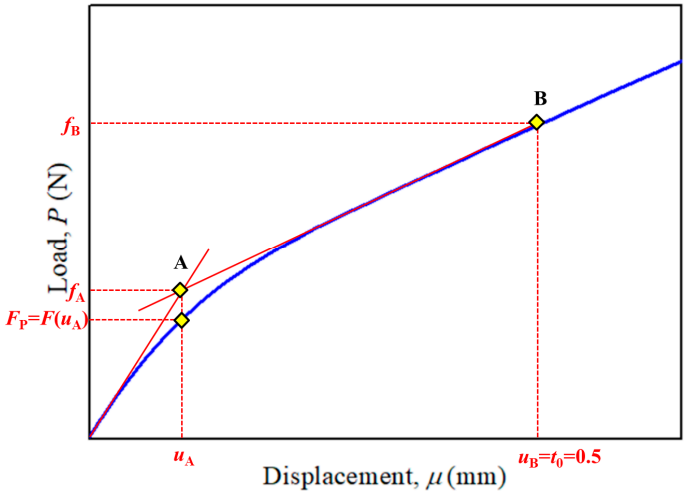

Figure 5. The method of extracting F_P proposed by the European Union Standard.

Error calculation formula:

$$err = \int_0^{u_B} [F(u) - f(u)]^2 du \quad (2)$$

As shown in Figure 5, the elastic and plastic stages of the SPT load–displacement curve were fitted. The initial fitting point of the data in stage I was set at (0, 0), and the end point of the data fitting in stage II was u_B (generally the standard thickness of the sample, i.e., 0.5 mm). The two fitting lines intersected to obtain an intersection point. The horizontal coordinate of the intersection point is u_A, making a line $x = u_A$, which intersected the load–displacement curve. In this case, the abscissa of the intersection point is the yield load of the load–displacement curve; that is, $F_P = F(u_A)$.

3.2. Hydrogen Embrittlement Sensitivity Analysis by Small Punch Test

In the quantitative analysis of HE sensitivity, the small-sized sample can not only shorten the hydrogen charging time, but also facilitates the hydrogen charging and discharging test in different hydrogen environments. As reported, it often takes ten or even dozens of hours for conventional tensile samples to reach hydrogen saturation concentration during electrolytic hydrogen charging, and a long-time test is needed if multiple samples are to be performed. The efficiency of hydrogen charging can be improved by using SPT and multiple samples can be tested at the same time. Thus, the time of hydrogen diffusion inside the sample is shortened, and the time hydrogen content takes to reach saturation is also reduced. An in situ small punch test setup with application of a high-pressure hydrogen environment and a low temperature reported by Shin et al. [49] is shown in Figure 6. Their recently published results prove the high applicability of studying HE susceptibility by using the small punch test. It not only ensures the accuracy of testing results, but also simplifies the consumption of the experiment.

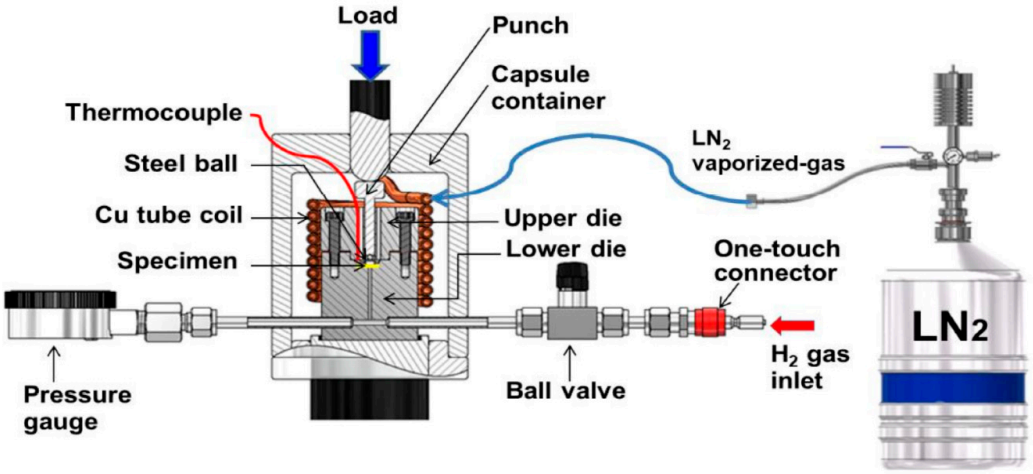

Figure 6. An in situ small punch test setup applying a high-pressure hydrogen environment and a low temperature (reprinted from Ref. [49]).

The Hydrogen Embrittlement Index (HEI) is a quantitative parameter used to evaluate the hydrogen embrittlement sensitivity. For standard samples, the change rate of elongation and reduction in the area in hydrogen-containing environments and non-hydrogen-containing environments is usually calculated to determine the HEI. The greater the change rate, the greater the hydrogen embrittlement sensitivity. However, SPT tests do not have clear quantitative indicators of elongation and area reduction. Generally, reduction of thickness (ROT) and relative reduction of thickness (RRT) are used to characterize HEI [50].

$$\mathrm{ROT} = \frac{t_0 - t_f}{t_0}, \quad \mathrm{RRT} = \frac{\mathrm{ROT}^{\mathrm{Hydrogen}}}{\mathrm{ROT}^{\mathrm{Air/N_2}}} \tag{3}$$

where t_0 is the initial specimen thickness and t_f is the final specimen thickness at failure.

Due to the difference between the load–displacement curve obtained via SPT and the standard stress–strain curve, the mechanical properties of the material cannot be obtained directly from the load–displacement curve of the SPT. The correlation methods of determining yield strength, tensile strength, elongation and area reduction are briefly introduced here, and are schematically shown in Figure 7. Researchers have put forward different theories to enrich and improve the method of associating SPT with traditional uniaxial tensile results. Through a large number of tests, the correlation formulae of yield strength σ_y and σ_{us} between SPT with the tensile test results are, respectively, obtained as follows [37–39]:

$$\sigma_y = \alpha_1 \frac{F_P}{t^2} + \alpha_2 \tag{4}$$

$$\sigma_{\mathrm{us}} = \beta_1 \frac{F_{max}}{t^2} + \beta_2 \tag{5}$$

where α_1, α_2, β_1 and β_2 are the correlation material constants, t is the specimen thickness, F_P is the determined yield load, and F_{max} is the maximum load.

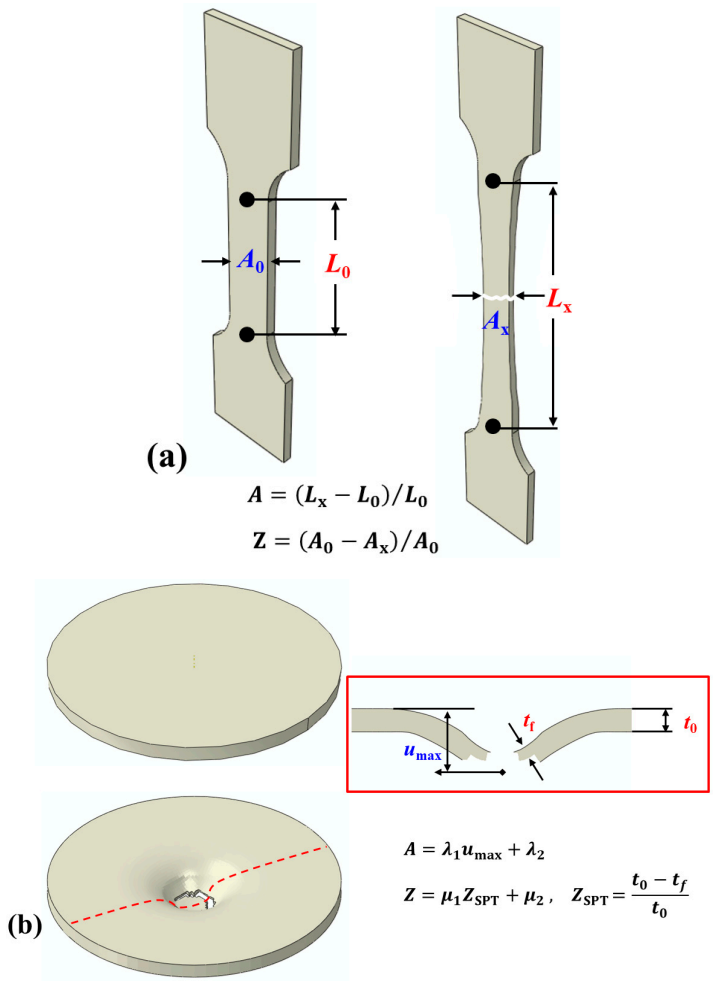

Figure 7. Schematic diagram of correlation between elongation and area reduction of (**a**) uniaxial tensile and (**b**) small punch specimen after fracture. (The dotted line is the imaginary section of a cutting plane. The cut cross-section is presented in the red frame, where the characteristic parameters are marked with a limited distance of arrows).

In addition to strength, the elongation (A) and area reduction (Z) also need to be considered. A commonly used method is to correlate the maximum axial displacement $u_{\max}$ of the sample center point with the post-fracture elongation (A) of the uniaxial tensile material. According to the percentage of the ratio of the maximum reduction ($t - t_f$) in the specimen thickness after fracture to the original thickness (t_0), the area reduction Z is associated, namely:

$$A = \lambda_1 u_{max} + \lambda_2 \tag{6}$$

$$Z = \mu_1 Z_{\mathrm{SPT}} + \mu_2, \qquad Z_{\mathrm{SPT}} = \frac{t_0 - t_{\mathrm{f}}}{t_0} \tag{7}$$

where λ_1, λ_2, μ_1, μ_2 are correlation material constants and $u_{\max}$ is the maximum axial displacement.

The mechanical performances without and with the hydrogen effect of several metallic materials tested via small punch tests are listed in Table 1. The calculated results are based on recently published papers [50–52]. Instead of the used area reduction and ductility loss in tensile testing results, the ROT and RRT are employed to quantitatively analyze HEI. The results show the fitness for the application of SPT to evaluate the hydrogen embrittlement damage. Among the listed materials, 316L steel presents the lowest hydrogen embrittlement sensitivity under the environment of 10 MPa hydrogen pressure. In addition, the values

of ROT and RRT are related to the displacement rate. With the decrease in displacement rate, the ROT and RRT gradually decrease, indicating higher susceptibility to hydrogen embrittlement.

Table 1. HE performance of several metallic materials tested via SPT.

Material	Punch Velocity v (mm/min)	Maximum Load F_{max} (N)	Fracture Displacement u_f (mm)	ROT (%)	RRT (%)	Environment
SA372 [50,52]	1.0	2487	2.01	50.57	/	N_2 (10 MPa)
	1.0	1487	1.08	23.92	47.37	
	0.1	1277	1.01	22.05	44.82	H_2 (10 MPa)
	0.01	976	0.96	15.43	30.81	
STS304 [50,52]	1.0	3128	2.68	55.52	/	N_2 (10 Mpa)
	1.0	1207	1.38	22.41	40.17	
	0.1	953	1.13	19.86	35.59	H_2 (10 MPa)
	0.01	905	1.12	18.85	34.07	
STS316L [51]	1.0	2796	2.48	/	/	N_2 (10 MPa)
	1.0	2121	1.81	/	99~100	
	0.1	1960	1.80	/	99~100	H_2 (10 MPa)
	0.01	1659	1.67	/	99~100	
24.5 wt% Mn [50]	1.0	3572	2.284	44.91	/	N_2 (10 MPa)
	1.0	1288	1.16	21.05	47.17	
	0.1	1038	0.87	16.16	35.77	H_2 (10 MPa)
	0.01	794	0.80	16.14	35.75	
9% Ni [50]	1.0	2688	2.30	60.42	/	N_2 (10 MPa)
	1.0	1720	1.23	28.11	47.26	
	0.1	1643	1.18	28.09	47.23	H_2 (10 MPa)
	0.01	1379	1.10	24.02	40.89	

Besides the above-mentioned ROT and RRT, G.'Alvarez et al. [53] proposed fracture energy (W_{SPT}), equivalent biaxial deformation at failure (ε_{qf}), and the rate of change of fitted circle to failure shape (Φ_{qf}) to characterize HEI. The method of fitting the diameter of the specimen to form a crack is shown in Figure 8 and the HE indexes of 42CrMo steel characterized by various calculation methods are listed in Table 2. Unlike in the results presented in Table 1, the electrochemical hydrogen charging method is performed. The three recommended methods by using W_{SPT}, ε_{qf} and Φ_{qf} are able to measure the HEI. The values of HEI increase with the decreased displacement rate and increased electrochemical charging density, which indicates an increased hydrogen concentration. The multiple measurement shows a more comprehensive method of quantifying the environmental damage.

HEI based on SPT fracture energy change rate is as follows:

$$HEI_{WSPT} = \frac{W_{SPT}^{\text{Air}}/t_0^2 - W_{SPT}^{\text{Hydrogen}}/t_0^2}{W_{SPT}^{\text{Air}}/t_0^2}, \quad W_{SPT} = \int_0^{u_{F\max}} F_u du \tag{8}$$

HEI based on SPT biaxial equivalent breaking strain change rate characterization is expressed as follows:

$$HEI_{\varepsilon qf} = \frac{\varepsilon_{qf}^{\text{Ajr}} - \varepsilon_{qf}^{\text{Hydrogen}}}{\varepsilon_{qf}^{\text{Ajr}}}, \qquad \varepsilon_{qf} = \ln(\frac{t_0}{t_f}) \tag{9}$$

HEI based on the characterization of the crack diameter change rate formed by sample breakage is expressed as follows:

$$HEI_{\Phi qf} = \frac{\Phi_{qf}^{\mathrm{Ajr}} - \Phi_{qf}^{\mathrm{Hydrogen}}}{\Phi_{qf}^{\mathrm{Ajr}}} \tag{10}$$

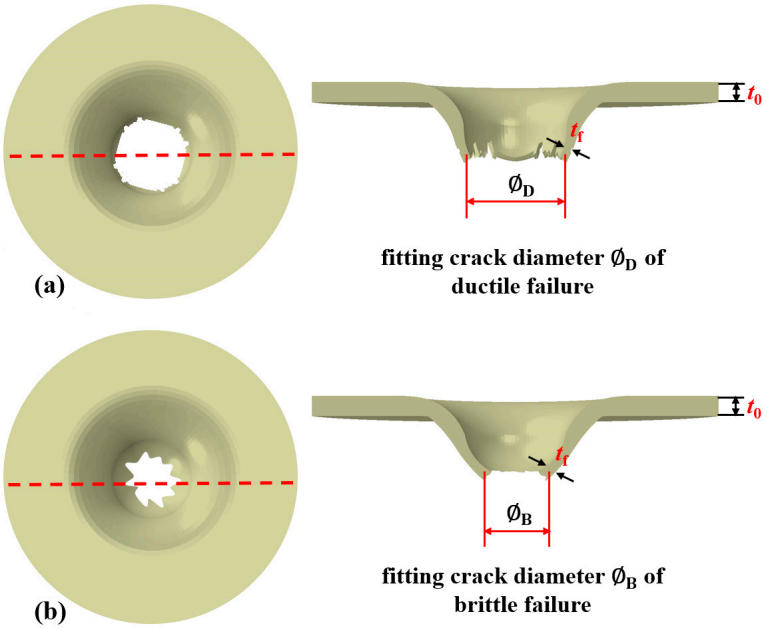

Figure 8. Schematic diagrams of small punch samples. (**a**) Ductile failure, (**b**) brittle failure.

Table 2. HE index of 42CrMo steel characterized via SPT (date from Ref. [53]).

Punch Velocity v (mm/min)	Maximum Load F_{max} (N)	Maximum Displacement u_{max} (mm)	Fracture Thickness t_f (mm)	HE Index			Environment
				HEI_{WSPT}	$HEI_{\varepsilon qf}$	$HEI_{\Phi qf}$	
0.2	1764	1.54	0.158	/	/	/	Uncharged
0.26	1600	1.30	0.224	19.85	30.01	14.29	
0.2	1630	1.37	0.254	27.14	42.88	15.71	
0.14	1418	1.12	0.316	47.34	60.07	17.99	Electrochemically charged 0.5 mA/cm^2
0.08	1211	1.00	0.392	57.90	85.17	24.53	
0.02	1015	0.91	0.479	64.58	94.44	35.98	
0.002	709	0.61	0.356	79.63	90.04	41.32	
0.001	582	0.57	0.406	85.21	93.52	45.50	
0.26	1616	1.35	0.258	25.07	42.88	16.32	
0.2	1346	1.11	0.346	51.00	68.25	17.99	
0.14	1362	1.12	0.376	52.58	78.15	21.16	Electrochemically charged 1 mA/cm^2
0.08	1078	0.91	0.393	66.30	79.32	26.68	
0.02	826	0.80	0.423	71.15	95.37	38.10	
0.002	639	0.62	0.408	81.71	95.44	43.92	
0.001	683	0.57	0.396	84.75	92.60	44.29	

4. Nanoindentation Test and Hydrogen-Induced Micro Property Evaluation

4.1. Nanoindentation Theory

Understanding the interaction between hydrogen and dislocation in metals is an important basis for perfecting the hydrogen embrittlement theory, and the key in this regard is the Nanoindentation (NI) testing method. The basic test principle of NI is based on the elastic contact theory proposed by Oliver–Pharr [54,55]. By recording the load–displacement curve during the whole process of the indenter pressing into the material, the characteristic parameters are obtained, and the nano-hardness and elastic modulus of

the test sample are calculated. The indenting test usually adopts a Berkovich indenter, and the nano-hardness (H) and elastic modulus (E) obtained through the test can be calculated using the following formulae:

$$H = \frac{P_{max}}{A_c} \tag{11}$$

$$E_{\mathrm{r}} = \frac{\sqrt{\pi}S}{2\sqrt{A_c}} \tag{12}$$

$$\frac{1}{\mathrm{E_r}} = \frac{1-v^2}{E} + \frac{1-\nu_{\mathrm{i}}^2}{E_i} \tag{13}$$

$$A_c = C_0 {h_c}^2 + C_1 h_c + C_2 h_c^{\frac{1}{2}} + C_3 h_c^{\frac{1}{4}} + C_4 h_c^{\frac{1}{8}} + C_5 h_c^{\frac{1}{16}} \tag{14}$$

where H is the nano-hardness, P_{max} is the maximum force, E_r is the reduced modulus, E is the elastic modulus, S is the contact stiffness of the initial unloading curve defined by $\mathrm{d}P/\mathrm{d}h$, P is the load force and h is the displacement, $E_{\mathrm{i}} = 1140\mathrm{GPa}$ and $\nu_{\mathrm{i}} = 0.07$ are the elastic modulus and Poisson's ratio of the diamond Berkovich indenter, respectively; A_c is the contact area and h_c is the contact depth.

4.2. Hydrogen-Induced Micro Property Evaluation Based on Nanoindentation

It is shown that hydrogen can affect the load–displacement curve obtained via the nanoindentation experiment, so that the effect of the change in hydrogen on the mechanical properties of the microstructure can be characterized. To date, much research on the effect of indentation on various materials in a hydrogen environment has been reported. From the perspective of characterizing the mechanical property evolutions of hydrogen effect, Zhang et al. [56–58] studied the influence of the indentation strain rate on the test results of mechanical properties of austenitic stainless steel under a hydrogen environment. Under the same test load condition, the displacement depth of indentation into 310S material decreased after hydrogen filling; that is, the nanoscale hardness value increased, and the material became hydrogen-hardened. Barnoush et al. [59–61] studied the effect of hydrogen on the ferrite phase and austenite phase plasticity and nano-hardness of duplex stainless steel via an in situ electrochemical hydrogen filling nanoindentation method. It was found that the hydrogen hardening degree of the austenite phase after hydrogen charging was higher than that of the ferrite phase [62].

Figure 9 shows nanoindentation load–displacement curves and scanning probe microscopies of 316L stainless steel under electrochemical charging with cathodic and andic potential. It can be clearly seen that hydrogen can reduce the load of the material when Pop-in occurs for the first time in the nanoindentation test. The load of Pop-in can be correlated with the driving force of dislocation nucleation. Based on the pure elasticity of the indentation segment, the driving force that nucleates a dislocation can be assumed to be the maximum shear stress τ_{max}. According to Hertzian elasticity theory, τ_{max} can be expressed as [57,63]:

$$P = \frac{4}{3} E_r R^{\frac{1}{2}} h^{\frac{3}{2}} \tag{15}$$

$$\tau_{\mathrm{max}} = 0.31 \left(\frac{6 {E_r}^2}{\pi^3 R^2} P \right)^{1/3} \tag{16}$$

where P is the indentation force, E_r is the reduced modulus, R is the indentation tip radius, and h is the indentation depth.

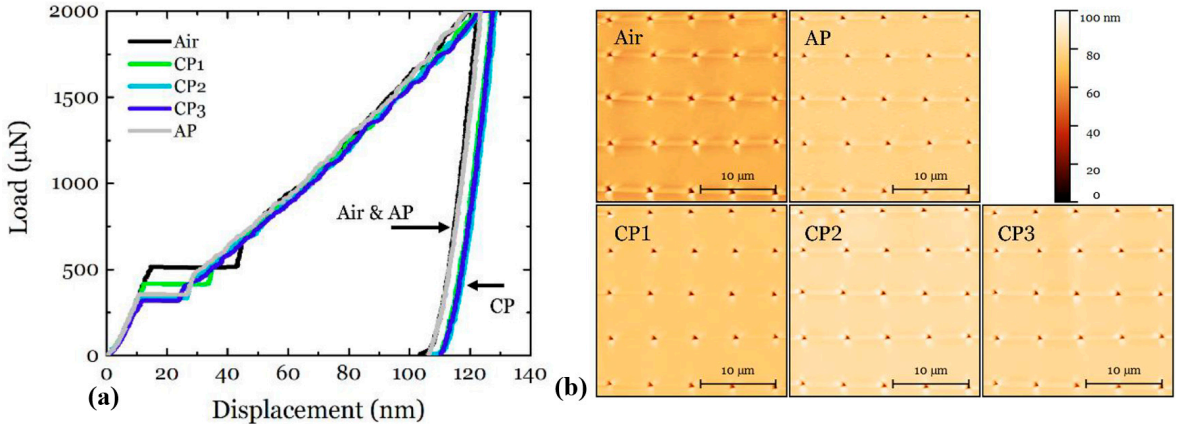

Figure 9. (**a**) Nanoindentation load–displacement curves and (**b**) scanning probe microscopies of 316L stainless steel under different electrochemical charging conditions (reprinted from Ref. [64]).

On the other hand, the interaction of hydrogen with the dislocation also depends on the strain rate. In the nanoindentation test, the indentation strain rate can be approximated as [65]:

$$\varepsilon = \frac{\dot{h}}{h} = \frac{1}{2}\left(\frac{\dot{P}}{P} - \frac{\dot{H}}{H}\right) \approx \frac{1}{2}\frac{\dot{P}}{P} \tag{17}$$

where h is the displacement, $\dot{h}$ is the displacement rate, P is the load, $\dot{P}$ is the loading rate, H is the hardness, and $\dot{H}$ is the hardness rate.

According to Orowan's equation, the strain rate affects the density and velocity of the moving dislocation, which can be expressed as [66]:

$$\dot{\varepsilon} = \rho_m b v \tag{18}$$

where $\dot{\varepsilon}$ is the strain rate, ρ_m is the mobile dislocation, b is the magnitude of the Burgers vector and v is the dislocation velocity.

In the case of a low strain rate, hydrogen is easily transferred by moving dislocation. The increase in hydrogen transport leads to an increase in dislocation activity at some local locations due to the enhanced ductility of hydrogen. At the same time, the increase in dislocation activity enhances the hydrogen transport effect. Therefore, the strain rate affects the interaction of hydrogen with the dislocation. Only when the dislocation velocity is less than the critical rate (v_c) will hydrogen move with the dislocation. According to dislocation theory, the critical rate v_c can be expressed as [58]:

$$v_c = \frac{DE}{30kTb} \tag{19}$$

Combining Equations (18) and (19), we can obtain:

$$\dot{\varepsilon} = \rho_m \frac{DE}{30kT} \tag{20}$$

where D is the hydrogen diffusivity; E is the dislocation trap biding energy; k is the Boltzmann constant; T is temperature.

5. Conclusions and Outlook

In recent decades, hydrogen embrittlement mechanism analysis and sensitivity evaluation have been hot topics at the forefront of research. With the development of hydrogen energy technology, many efforts have been made to design safe, durable, and low-cost storage tanks and pipelines. Quantitative analysis of the hydrogen influence on the mechanical properties of materials is one of the crucial issues that can ensure the structural integrity of

hydrogen energy equipment. The conventional-sized specimen testing methods are very mature. However, the regular-sized sample is not suitable for evaluating the damage of core components of limited size, such as nozzles and valves. Hence, the micro-sample testing technology helps to further evaluate the system of hydrogen embrittlement damage. In the latest research, combined analyses including macro-, meso-, and micro-scale tests have been successfully performed, providing more comprehensive experimental proof and deeper insights.

Compared with conventional-sized samples, micro-sized sample testing faces greater challenges in specimen preparation and data correlation. The specimen size effect and data incomparability are the two most important and unavoidable factors. With the decrease in the sample size, the size effect phenomenon—that is, the test result—deviates from the macroscopic intrinsic mechanical behavior of the measured material, which becomes more obvious. The data incomparability is usually caused by the difference in stress state or strain path caused by the geometric dissimilarity between standard and small samples. With the advancement of processing technology and intelligent algorithms, the impact of external factors on testing results and analysis will progressively reduce, and the further application issues of small sample testing technology are as follows:

(1) Fatigue performance. There are few reported studies on the fatigue properties of small-sized samples. The commonly used small round bar fatigue sample mainly includes hourglass-type and equal section-type specimens, during which the equal section specimens show more reliable experimental results. The small punch test and nanoindentation test are mainly used to characterize the mechanical property evolution under cyclic loading, which is still unable to accurately obtain the fatigue life and fatigue strength. At present, researchers have been exploring the creep-fatigue test using the small punch test, which will inspire the investigation on fatigue damage evolution in a hydrogen environment.

(2) Ultra-small specimen testing requirement. With the continuous requirements of testing technology improvement, the sample size has begun to develop towards a more miniaturized direction, e.g., specimens employed in the micro-pillar compression test, micro-cantilever bending test and environmental in situ transmission electron microscope test. The ultra-small specimen test facilitates the observation of mechanical phenomena at a smaller scale, even at nano-scale.

(3) High-throughput testing system. The development of the high-throughput testing system is significant for the new-generation materials genetic engineering strategy. Due to the advantage of its limited sample size, the multi-extensive mechanical properties are easier to achieve through one experiments involving one micro-sample test, compared with the standard specimen test. The recommended model of rational design, efficient experiment and big data analytics can accelerate the discovery of new materials and further widen the model's applications. Such a system can significantly accelerate the study on fitness for the service of different materials under the hydrogen environment.

Author Contributions: Conceptualization, P.T. and W.Z.; methodology, P.T. and X.M.; software, P.T. and W.Z.; validation, P.T., X.M. and J.P.; formal analysis, P.T. and W.Z.; investigation, P.T. and W.Z.; resources, P.T. and W.Z.; data curation, P.T., W.Z. and J.P.; writing—original draft preparation, P.T. and W.Z.; writing—review and editing, P.T. and W.Z.; visualization, P.T., X.M. and J.P.; supervision, P.T., X.M., J.P. and W.L.; project administration, P.T., X.M., J.P. and W.L.; funding acquisition, P.T. All authors have read and agreed to the published version of the manuscript.

Funding: The authors gratefully acknowledge the financial support of the National Natural Science Foundation of China (52205142), Natural Science Research of Jiangsu Higher Education Institutions of China (22KJB460012).

Conflicts of Interest: The authors declare that they have no known competing financial interest or personal relationships that could have appeared to influence the work reported in this paper.

References

1. Wasim, M.; Djukic, M.B. Hydrogen embrittlement of low carbon structural steel at macro-, micro-and nano-levels. *Int. J. Hydrogen Energy* **2020**, *45*, 2145–2156. [CrossRef]
2. Chen, Y.; Zhao, S.; Ma, H.; Wang, H.; Hua, L.; Fu, S. Analysis of hydrogen embrittlement on aluminum alloys for vehicle-mounted hydrogen storage tanks: A review. *Metals* **2021**, *11*, 1303. [CrossRef]
3. Wu, X.; Zhang, H.; Yang, M.; Jia, W.; Qiu, Y.; Lan, L. From the perspective of new technology of blending hydrogen into natural gas pipelines transmission: Mechanism, experimental study, and suggestions for further work of hydrogen embrittlement in high-strength pipeline steels. *Int. J. Hydrogen Energy* **2022**, *47*, 8071–8090. [CrossRef]
4. Ustolin, F.; Paltrinieri, N.; Berto, F. Loss of integrity of hydrogen technologies: A critical review. *Int. J. Hydrogen Energy* **2020**, *45*, 23809–23840. [CrossRef]
5. Campari, A.; Ustolin, F.; Alvaro, A.; Paltrinieri, N. A review on hydrogen embrittlement and risk-based inspection of hydrogen technologies. *Int. J. Hydrogen Energy* 2023, *in press*. [CrossRef]
6. Zhu, H.; Pan, Q.; Zhang, K.; Zhou, C.; Zhang, W.; Yao, Y.; Zhang, L. The difference in fatigue crack growth induced by internal and external hydrogen in selective laser melted 304L stainless steel. *Int. J. Fatigue* **2022**, *163*, 107052. [CrossRef]
7. Khare, A.; Vishwakarma, M.; Parashar, V. A review on failures of industrial components due to hydrogen embrittlement & techniques for damage prevention. *Int. J. Appl. Eng. Res.* **2017**, *12*, 1784–1792.
8. Li, X.; Ma, X.; Zhang, J.; Akiyama, E.; Wang, Y.; Song, X. Review of hydrogen embrittlement in metals: Hydrogen diffusion, hydrogen characterization, hydrogen embrittlement mechanism and prevention. *Acta Metall. Sin. (Engl. Lett.)* **2020**, *33*, 759–773. [CrossRef]
9. Nagumo, M. Mechanistic Aspects of Fracture I—Brittle Fracture Models. In *Fundamentals of Hydrogen Embrittlement*; Springer Nature: Singapore, 2023; pp. 245–263.
10. Wang, S.; Martin, M.L.; Sofronis, P.; Ohnuki, S.; Roberton, I.M. Hydrogen-induced intergranular failure of iron. *Acta Mater.* **2014**, *69*, 275–282. [CrossRef]
11. Katzarov, I.H.; Paxton, A.T. Hydrogen embrittlement II. Analysis of hydrogen-enhanced decohesion across (111) planes in α-Fe. *Phys. Rev. Mater.* **2017**, *1*, 033603. [CrossRef]
12. Birnbaum, H.K.; Sofronis, P. Hydrogen-enhanced localized plasticity—A mechanism for hydrogen-related fracture. *Mater. Sci. Eng. A* **1994**, *176*, 191–202. [CrossRef]
13. Martin, M.L.; Dadfarnia, M.; Nagao, A.; Wang, S.; Sofronis, P. Enumeration of the hydrogen-enhanced localized plasticity mechanism for hydrogen embrittlement in structural materials. *Acta Mater.* **2019**, *165*, 734–750. [CrossRef]
14. Wasim, M.; Djukic, M.B.; Ngo, T.D. Influence of hydrogen-enhanced plasticity and decohesion mechanisms of hydrogen embrittlement on the fracture resistance of steel. *Eng. Fail. Anal.* **2021**, *123*, 105312. [CrossRef]
15. Lin, M.; Yu, H.; Ding, Y.; Wang, G.; Olden, V.; Alvaro, A.; He, J.; Zhang, Z. A predictive model unifying hydrogen enhanced plasticity and decohesion. *Scr. Mater.* **2022**, *215*, 114707. [CrossRef]
16. Nguyen, T.T.; Tak, N.; Park, J.; Nahm, S.H.; Beak, U.B. Hydrogen embrittlement susceptibility of X70 pipeline steel weld under a low partial hydrogen environment. *Int. J. Hydrogen Energy* **2020**, *45*, 23739–23753. [CrossRef]
17. Wang, C.; Zhang, J.; Liu, C.; Hu, Q.; Zhang, R.; Xu, X.; Yang, H.; Ning, Y.; Li, Y. Study on hydrogen embrittlement susceptibility of X80 steel through in-situ gaseous hydrogen permeation and slow strain rate tensile tests. *Int. J. Hydrogen Energy* **2023**, *48*, 243–256. [CrossRef]
18. Singh, D.K.; Raman RK, S.; Maiti, S.K.; Bhandakkar, T.K.; Pal, S. Investigation of role of alloy microstructure in hydrogen-assisted fracture of AISI 4340 steel using circumferentially notched cylindrical specimens. *Mater. Sci. Eng. A* **2017**, *698*, 191–197. [CrossRef]
19. Cayón, A.; Gutiérrez-Solana, F.; Arroyo, B.; Lvarez, J.A. Hydrogen embrittlement processes in microalloyed steel notched tensile samples. *Theor. Appl. Fract. Mech.* **2021**, *112*, 102878. [CrossRef]
20. Arniella, V.; Zafra, A.; Álvarez, G.; Rodriguez, C. Comparative study of embrittlement of quenched and tempered steels in hydrogen environments. *Int. J. Hydrogen Energy* **2022**, *47*, 17056–17068. [CrossRef]
21. Arniella, V.; Álvarez, G.; Belzunce, J.; Rodriguez, C. Hydrogen embrittlement of 2205 duplex stainless steel in in-situ tensile tests. *Theor. Appl. Fract. Mech.* **2023**, *124*, 103794. [CrossRef]
22. Nguyen, T.T.; Park, J.S.; Kim, W.S.; Nahm, S.H.; Beak, U.B. Environment hydrogen embrittlement of pipeline steel X70 under various gas mixture conditions with in situ small punch tests. *Mater. Sci. Eng. A* **2020**, *781*, 139114. [CrossRef]
23. Nguyen, T.T.; Park, J.S.; Nahm, S.H.; Beak, U.B. Evaluation of hydrogen related degradation of API X42 pipeline under hydrogen/natural gas mixture conditions using small punch test. *Theor. Appl. Fract. Mech.* **2021**, *113*, 102961. [CrossRef]
24. Lulu-Bitton, N.; Navi, N.U.; Rosen, B.A.; Haroush, S.; Sabatani, E.; Eretz-Kdosha, Y.; Agronov, G.; Eliaz, N. The influence of gaseous hydrogen charging on the microstructural and mechanical behavior of electron beam melted and wrought Ti–6Al–4V alloys using the small punch test. *Int. J. Hydrogen Energy* **2023**, *48*, 34077–34093. [CrossRef]
25. Wang, X.; Zhu, T.; Zhang, J.; Ding, H.; Xiao, S.; Lu, L.; Yang, B.; Yang, G.; Liu, Y. A review of selected small specimen test techniques for identifying deformation and failure properties of metallic materials. *J. Mater. Sci.* **2023**, *58*, 63–100. [CrossRef]
26. Zheng, P.; Chen, R.; Liu, H.; Chen, J.; Zhang, Z.; Liu, X.; Shen, Y. On the standards and practices for miniaturized tensile test—A review. *Fusion Eng. Des.* **2020**, *161*, 112006. [CrossRef]
27. Song, M.; Guan, K.; Qin, W.; Szpunar, J.A.; Chen, J. Size effect criteria on the small punch test for AISI 316L austenitic stainless steel. *Mater. Sci. Eng. A* **2014**, *606*, 346–353. [CrossRef]

28. Roach, A.M.; White, B.C.; Garland, A.; Jared, B.H.; Carroll., J.D.; Boyce, B.L. Size-dependent stochastic tensile properties in additively manufactured 316L stainless steel. *Addit. Manuf.* **2020**, *32*, 101090. [CrossRef]
29. Gussev, M.N.; Howard, R.H.; Terrani, K.A.; Field, K.G. Sub-size tensile specimen design for in-reactor irradiation and post-irradiation testing. *Nucl. Eng. Des.* **2017**, *320*, 298–308. [CrossRef]
30. Liu, H.; Chen, R.; Wen, M.; Zhang, L.; Shen, Y. Optimizing parallel section length for small tensile specimen with fabrication non-uniformity in thickness. *Fusion Eng. Des.* **2019**, *147*, 111244. [CrossRef]
31. Liu, H.; Shen, Y.; Yang, S.; Zhang, P.; Zhang, L. A comprehensive solution to miniaturized tensile testing: Specimen geometry optimization and extraction of constitutive behaviors using inverse FEM procedure. *Fusion Eng. Des.* **2017**, *121*, 188–197. [CrossRef]
32. Wan, D.; Deng, Y.; Barnoush, A. Hydrogen embrittlement effect observed by in-situ hydrogen plasma charging on a ferritic alloy. *Scr. Mater.* **2018**, *151*, 24–27. [CrossRef]
33. Depover, T.; Wan, D.; Wang, D.; Barnoush, A.; Verbeken, K. The effect of hydrogen on the crack initiation site of TRIP-assisted steels during in-situ hydrogen plasma micro-tensile testing: Leading to an improved ductility? *Mater. Charact.* **2020**, *167*, 110493. [CrossRef]
34. Mine, Y.; Koga, K.; Kraft, O.; Takashima, K. Mechanical characterisation of hydrogen-induced quasi-cleavage in a metastable austenitic steel using micro-tensile testing. *Scr. Mater.* **2016**, *113*, 176–179. [CrossRef]
35. Asadipoor, M.; Anaraki, A.P.; Kadkhodapour, J.; Sharifi, S.M.H.; Barnoush, A. Macro-and microscale investigations of hydrogen embrittlement in X70 pipeline steel by in-situ and ex-situ hydrogen charging tensile tests and in-situ electrochemical micro-cantilever bending test. *Mater. Sci. Eng. A* **2020**, *772*, 138762. [CrossRef]
36. Ueki, S.; Oura, R.; Mine, Y.; Takashima, K. Micro-mechanical characterisation of hydrogen embrittlement in nano-twinned metastable austenitic stainless steel. *Int. J. Hydrogen Energy* **2020**, *45*, 27950–27957. [CrossRef]
37. *GB/T 29459-2012*; Test Method for Small Punch Testing of Metallic Materials for In-Service Pressurized Equipment. China National Standardization Management Committee: Beijing, China, 2012.
38. *ASTM E3205-2020*; Standard Test Method for Small Punch Testing of Metallic Materials. ASTM International: Conshohocken, PA, USA, 2020.
39. *BS EN 10371-2021*; Metallic Materials—Small Punch Test Method. British Standards Institution: London, UK, 2021.
40. Li, K.; Peng, J.; Zhou, C. Construction of whole stress-strain curve by small punch test and inverse finite element. *Results Phys.* **2018**, *11*, 440–448. [CrossRef]
41. Geng, X.; Peng, J.; Jiang, L.; Liu, X.; Tu, Y.; Xue, Z. Experimental study of mechanical properties and fracture modes in different regions of the nickel-based welding joint based on small punch test. *Weld. World* **2023**, *67*, 637–650. [CrossRef]
42. Altstadt, E.; Bergner, F.; Houska, M. Use of the small punch test for the estimation of ductile-to-brittle transition temperature shift of irradiated steels. *Nucl. Mater. Energy* **2021**, *26*, 100918. [CrossRef]
43. Lai, H.S.; Jiang, X. Determination of fracture toughness through small punch test of notched-tube specimen. *Eng. Fract. Mech.* **2023**, *279*, 109059. [CrossRef]
44. Sun, W.; Li, M.; Wen, Z.; Zhou, G.; Yue, Z.; Tu, S. Uncertainties in and Recommendations to Small Punch Tensile and Creep Tests for Ductile Materials. *Eng. Fract. Mech.* **2023**, *289*, 109443. [CrossRef]
45. Lancaster, R.J.; Jeffs, S.P.; Haigh, B.J.; Barnard, N.C. Derivation of material properties using small punch and shear punch test methods. *Mater. Des.* **2022**, *215*, 110473. [CrossRef]
46. Leclerc, N.; Khosravani, A.; Hashemi, S.; Miracle, D.B.; Kalidindi, S.R. Correlation of measured load-displacement curves in small punch tests with tensile stress-strain curves. *Acta Mater.* **2021**, *204*, 116501. [CrossRef]
47. Peng, J.; Vijayanand, V.D.; Knowles, D.; Truman, C.; Mostafavi, M. The sensitivity ranking of ductile material mechanical properties, geometrical factors, friction coefficients and damage parameters for small punch test. *Int. J. Press. Vessel. Pip.* **2021**, *193*, 104468. [CrossRef]
48. *CWA 15627-2007*; Small Punch Test Method for Metallic Material. European Committee for Standardization: Brussels, Belgium, 2007.
49. Shin, H.S.; Yeo, J.; Baek, U.B. Influence of specimen surface roughness on hydrogen embrittlement induced in austenitic steels during in-situ small punch testing in high-pressure hydrogen environments. *Metals* **2021**, *11*, 1579. [CrossRef]
50. Bae, K.O.; Shin, H.S.; Baek, U.B. Quantitative evaluation of hydrogen embrittlement susceptibility in various steels for energy use using an in-situ small punch test. *Int. J. Hydrogen Energy* **2021**, *46*, 20107–20118. [CrossRef]
51. Shin, H.S.; Custodio, N.A.; Baek, U.B. Numerical analysis for characterizing hydrogen embrittlement behaviors induced in STS316L stainless steel using an in-situ small-punch test. *Theor. Appl. Fract. Mech.* **2021**, *116*, 103139. [CrossRef]
52. Shin, H.S.; Bae, K.O.; Baek, U.B.; Nahm, S.H. Establishment of an in-situ small punch test method for characterizing hydrogen embrit-tlement behaviors under hydrogen gas environments and new influencing factor. *Int. J. Hydrogen Energy* **2019**, *44*, 23472–23483. [CrossRef]
53. Álvarez, G.; Arniella, V.; Belzunce, F.J.; Rodriguez, C. Study of the influence of current density and displacement rate on hydrogen em-brittlement using small punch tests. *Theor. Appl. Fract. Mech.* **2023**, *125*, 103838. [CrossRef]
54. Oliver, W.C.; Pharr, G.M. An improved technique for determining hardness and elastic modulus using load and displacement sensing indentation experiments. *J. Mater. Res.* **1992**, *7*, 1564–1583. [CrossRef]

55. Oliver, W.C.; Pharr, G.M. Measurement of hardness and elastic modulus by instrumented indentation: Advances in understanding and refinements to methodology. *J. Mater. Res.* **2004**, *19*, 3–20. [CrossRef]
56. Hong, Y.; Zhou, C.; Zheng, Y.; Zhang, L.; An, B.; Chen, X.; Wang, X. Hydrogen effect on the deformation evolution process in situ detected by nanoindentation continuous stiffness measurement. *Mater. Charact.* **2017**, *127*, 35–40. [CrossRef]
57. Hong, Y.; Zhou, C.; Zheng, Y.; Zhang, L.; Zheng, J.; Chen, X. Effect of hydrogen and strain rate on nanoindentation creep of austenitic stainless steel. *Int. J. Hydrogen Energy* **2019**, *44*, 1253–1262. [CrossRef]
58. Hong, Y.; Zhou, C.; Zheng, Y.; Zhang, L.; Zheng, J.; Chen, X. Dependence of strain rate on hydrogen-induced hardening of austenitic stainless steel investigated by nanoindentation. *Int. J. Hydrogen Energy* **2019**, *44*, 14055–14063. [CrossRef]
59. Barnoush, A.; Zamanzade, M.; Vehoff, H. Direct observation of hydrogen enhanced plasticity in super duplex stainless steel by means of in situ electrochemical methods. *Scr. Mater.* **2010**, *62*, 242–245. [CrossRef]
60. Barnoush, A.; Vehoff, H. Recent developments in the study of hydrogen embrittlement: Hydrogen effect on dislocation nucleation. *Acta Mater.* **2010**, *58*, 5274–5285. [CrossRef]
61. Barnoush, A.; Asgari, M.; Johnsen, R. Resolving the hydrogen effect on dislocation nucleation and mobility by electrochemical nanoindentation. *Scr. Mater.* **2012**, *66*, 414–417. [CrossRef]
62. Kheradmand, N.; Johnsen, R.; Olsen, J.S.; Barnoush, A. Effect of hydrogen on the hardness of different phases in super duplex stainless steel. *Int. J. Hydrogen Energy* **2016**, *41*, 704–712. [CrossRef]
63. Basa, A.; Wang, D.; Espallargas, N.; Wan, D. An in-situ electrochemical nanoindentation (ECNI) study on the effect of hydrogen on the mechanical properties of 316L austenitic stainless steel. *Materials* **2021**, *14*, 6426. [CrossRef]
64. Hong, Y.; Zhou, C.; Zheng, Y.; Zhang, L.; Chen, X. Hydrogen effect on nanoindentation creep of austenitic stainless steel: A comparative study between primary creep stage and steady-state creep stage. *Int. J. Hydrogen Energy* **2019**, *44*, 22576–22583. [CrossRef]
65. Lucas, B.N.; Oliver, W.C. Indentation power-law creep of high-purity indium. *Metall. Mater. Trans. A* **1999**, *30*, 601–610. [CrossRef]
66. Durst, K.; Maier, V. Dynamic nanoindentation testing for studying thermally activated processes from single to nanocrystalline metals. *Curr. Opin. Solid State Mater. Sci.* **2015**, *19*, 340–353. [CrossRef]